



HAL
open science

The origin of the LMC stellar bar: clues from the SFH of the bar and inner disc

L. Monteagudo, C. Gallart, M. Monelli, E. J. Bernard, P. B. Stetson

► To cite this version:

L. Monteagudo, C. Gallart, M. Monelli, E. J. Bernard, P. B. Stetson. The origin of the LMC stellar bar: clues from the SFH of the bar and inner disc. *Monthly Notices of the Royal Astronomical Society: Letters*, 2018, 473, pp.L16-L20. 10.1093/mnrasl/slx158 . insu-03689242

HAL Id: insu-03689242

<https://insu.hal.science/insu-03689242>

Submitted on 7 Jun 2022

HAL is a multi-disciplinary open access archive for the deposit and dissemination of scientific research documents, whether they are published or not. The documents may come from teaching and research institutions in France or abroad, or from public or private research centers.

L'archive ouverte pluridisciplinaire **HAL**, est destinée au dépôt et à la diffusion de documents scientifiques de niveau recherche, publiés ou non, émanant des établissements d'enseignement et de recherche français ou étrangers, des laboratoires publics ou privés.

The origin of the LMC stellar bar: clues from the SFH of the bar and inner disc

L. Monteagudo,^{1,2★} C. Gallart,^{1,2} M. Monelli,^{1,2} E. J. Bernard³ and P. B. Stetson⁴

¹*Instituto de Astrofísica de Canarias (IAC), Calle Vía Láctea s/n, E-38205 La Laguna, Tenerife, Spain*

²*Departamento de Astrofísica, Universidad de La Laguna (ULL), E-38206 La Laguna, Tenerife, Spain*

³*Université Côte d'Azur, OCA, CNRS, Lagrange, F-06304 Nice, France*

⁴*Herzberg Astronomy and Astrophysics, National Research Council Canada, 5071 West Saanich Road, Victoria, BC V9E 2E7, Canada*

Accepted 2017 September 26. Received 2017 September 26; in original form 2017 July 29

ABSTRACT

We discuss the origin of the Large Magellanic Cloud (LMC) stellar bar by comparing the star formation histories (SFHs) obtained from deep colour–magnitude diagrams (CMDs) in the bar and in a number of fields in different directions within the inner disc. The CMDs, reaching the oldest main-sequence turn-offs in these very crowded fields, have been obtained with VIMOS on the Very Large Telescope in the service mode, under very good seeing conditions. We show that the SFHs of all fields share the same patterns, with consistent variations of the star formation rate as a function of time in all of them. We therefore conclude that no specific event of star formation can be identified with the formation of the LMC bar, which instead likely formed from a redistribution of disc material which occurred when the LMC disc became bar unstable, and shared a common SFH with the inner disc thereafter. The strong similarity between the SFH of the centre and edge of the bar rules out the expected significant spatial variations of the SFH across the bar.

Key words: Hertzsprung–Russell and colour–magnitude diagrams – galaxies: evolution – Magellanic Clouds – galaxies: stellar content – galaxies: structure.

1 INTRODUCTION

The Large Magellanic Cloud (LMC) is the prototype of a whole class of galaxies, the Barred Magellanic Spirals (SBm), characterized by the presence of an optically visible stellar bar, coincident or not with the dynamical centre of the galaxy, a single spiral arm emanating from an end of the bar, and often, a large star-forming region at one end of the bar (de Vaucouleurs & Freeman 1972).

The true nature of the bars in these late-type galaxies is the subject of controversy. While in early-type spirals, the barred optical morphology is also evident in both the distribution and kinematics of the neutral H₁ gas, this is not always the case in SBm; in many examples, the bar seems to have a modest effect (if any) on the gas kinematics towards the centre of the galaxy (Wilcots 2008).

The existence of the LMC as a very nearby representative of the SBm class offers an excellent opportunity to gain insight about the origin and evolution of these barred structures. In the LMC, a stellar bar is clearly visible in near-IR maps and stellar density contours (e.g. Cioni, Habing & Israel 2000; van der Marel 2001) but is not apparent in the H₁ gas disc (Kim et al. 1998; Staveley-Smith et al. 2003) and is not the site of current star formation as

shown by H α images (Kim et al. 1999). There has been a fair amount of discussion regarding its three-dimensional structure (e.g. Zhao & Evans 2000; Zaritsky 2004) and its location with respect to the stellar disc (Subramaniam 2003; Nikolaev et al. 2004; Lah, Kiss & Bedding 2005; Koerwer 2009; Subramaniam & Subramanian 2009).

A few studies have addressed the star formation history (SFH) of the LMC bar and nearby fields. The high stellar density in the centre of the bar, however, has made it difficult to obtain colour–magnitude diagrams (CMDs) reaching the oldest main-sequence turn-offs (oMSTO) with ground-based telescopes, necessary for a reliable determination of the SFH for all ages. The WFPC2 on *Hubble Space Telescope* (HST) produced the first very deep CMDs of fields in the LMC bar (Elson, Gilmore & Santiago 1997; Holtzman et al. 1999; Olsen 1999; Smecker-Hane et al. 2002; Weisz et al. 2013), which were populated enough to lead to reliable SFHs; but these were for small portions of the bar and were thus potentially affected by local fluctuations in the stellar populations. Deep and well-populated CMDs of the inner LMC disc immediately surrounding the bar region were even more challenging, because a single WFPC2 field typically produced very sparse CMDs. To address this issue, some programmes observed mosaics of several WFPC2 fields in the inner LMC disc in different directions from the bar centre, and produced CMDs as populated as those in the bar (Smecker-Hane et al. 2002).

* E-mail: laram@iac.es

Comprehensive coverage of the LMC bar and inner disc using the *HST*, however, remains unfeasible.

For this reason, we have adopted an alternative approach using ground-based observations, taken in excellent seeing conditions with the VLT in the service mode. This strategy produces CMDs reaching the oMSTO even in the centre of the LMC bar and allows us to study representative portions of the inner LMC for the first time, leading to sound conclusions on their entire SFH. As part of a larger project devoted to an in-depth study of the central LMC SFH and its spatial variations, in this Letter, we show how the striking similarity of the SFHs of a number of bar and disc fields puts strong constraints on the formation of the LMC bar. This has obvious importance for addressing the long-standing issue regarding the nature of the LMC bar and its possibly differentiated formation and/or evolution.

2 OBSERVATIONS AND DATA REDUCTION

We have used the Visible Multi-Object Spectrograph (VIMOS) on the Very Large Telescope (VLT) to obtain deep *B* and *R* images in the central part of the LMC. The camera has four CCDs, each with a $7 \text{ arcmin} \times 8 \text{ arcmin}$ field of view. We observed a total of 11 fields in order to have a significant sampling of the LMC's innermost region. Two fields probe the LMC bar, and the remaining nine fields are distributed in a ring in the inner disc and northern arm within a distance of $R < 3.2$ from the bar centre. Fig. 1 shows the location of these VIMOS fields, superimposed on a stellar density map of the LMC based on data from the *Gaia* DR1 (Gaia Collaboration et al. 2016).

The observations were designed to reach the oMSTO in the CMD, necessary to obtain a reliable full lifetime SFH. They were taken in service mode to ensure the good seeing $\simeq 0.6 \text{ arcsec} - 0.8 \text{ arcsec}$ necessary to resolve stars down to a faint magnitude limit in these very crowded areas.

We obtained the photometry using DAOPHOT IV and ALLFRAME (Stetson 1987, 1994). Each chip of each image was reduced independently. Photometric calibration is based on a number of standard fields observed during a photometric campaign with the CTIO Blanco Telescope, with the MOSAIC camera, on 2010 January 15. In this period, we observed the same 11 fields and a number of standard fields, which were selected because of the large number of

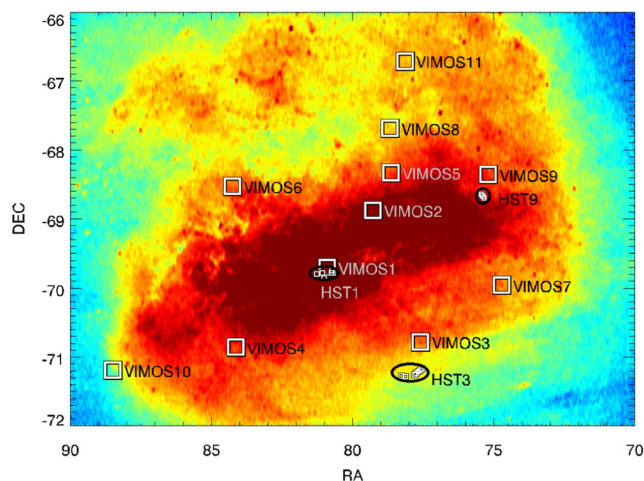


Figure 1. Stellar density map of the central region of the LMC, based on the photometry of the *Gaia* Data Release 1. The location of our VIMOS fields and the archival *HST* pointings are overlaid.

standard stars available in the data base of P.B. Stetson.¹ Finally, a large number of artificial-star tests were performed in each frame following the procedure described in Gallart et al. (1999). These are used both to derive completeness factors and to model photometric errors in the synthetic CMD.

To facilitate the comparison of our SFHs with previous work, we have supplemented our ground-based data with deep archival *HST* imaging. These *HST* data are based on WFPC2 images from several programmes: GO7382 and GO8576 (P.I. Smecker-Hane), GO7306 (P.I. Cook) and GO6229 (P.I. Trauger). We used photometry and artificial-star tests ($\sim 1.2 \times 10^5$ per field) taken from the Local Group Stellar Photometry Archive² (LGSPA: Holtzman, Afonso & Dolphin 2006). Fig. 1 shows that the mosaics of disc WFPC2 fields and several WFPC2 fields in the bar are clustered in three small regions of the LMC, which are very close to three of our fields, namely VIMOS1, VIMOS3 and VIMOS9. We have combined the *HST* observations in three CMDs which we will call *HST1*, *HST3* and *HST9* to indicate their closeness to a VIMOS field.

Fig. 2 shows a sample of the VIMOS (left-hand panels) and *HST* (right-hand panels) CMDs, for the central bar field (VIMOS1 and *HST1* on the top) and one representative disc field (VIMOS3 and *HST3*). In the case of the bar fields, CMDs from a single WFPC2 pointing contain a number of stars which is sufficient for a robust determination of the SFH (Holtzman et al. 1999; Olsen 1999; Smecker-Hane et al. 2002). For the disc, *HST* GO programmes 7382 and 8576 (see Smecker-Hane et al. 2002) mosaicked 6–10 WFPC2 pointings to obtain CMDs with a number of stars comparable to that of a bar field. These *HST* CMDs are deeper than the VIMOS ones, but the latter have the advantage of containing a much larger number of stars (see Fig. 2).

An old isochrone has been superimposed on the ground-based CMD of the central bar field (top left panel of Fig. 2) to show that our goal to reach the oMSTO in the CMD was achieved in our most crowded field. To our knowledge, these are the only data taken from the ground with photometry deep enough to reach the oMSTO in the centre of the LMC bar. Fig. 2 also shows the *bundles*, or areas of the CMD which have been used to derive the SFH through comparison of the distribution of stars in the observed and synthetic CMDs (see Section 3.1). The number of stars inside the bundles has been labelled in each CMD. Note that, in spite of the fact that several WFPC2 fields have been combined to build the CMDs shown in Fig. 2, the number of stars in the VIMOS CMDs which are relevant for the SFH derivation is many times greater than in the WFPC2 CMDs.

3 THE STAR FORMATION HISTORY

3.1 SFH derivation

The SFH calculations for both VIMOS and WFPC2 data were carried out using the CMD-fitting technique, in a way very similar to that described in Aparicio & Hidalgo (2009) and Meschin et al. (2014). We used IAC-star³ (Aparicio & Gallart 2004) to compute a synthetic CMD with a constant star formation rate (SFR(*t*)) between 13.5 and $\simeq 0.03$ Gyr ago; 5×10^7 stars in the whole age range are uniformly distributed between $Z = 0.0001$ and

¹ <http://www3.cadc-ccda.hia-ihh.nrc-cnrc.gc.ca/community/STETSON/standards/>

² <http://astronomy.nmsu.edu/holtz/archival/html/lg.html>

³ <http://iac-star.iac.es>

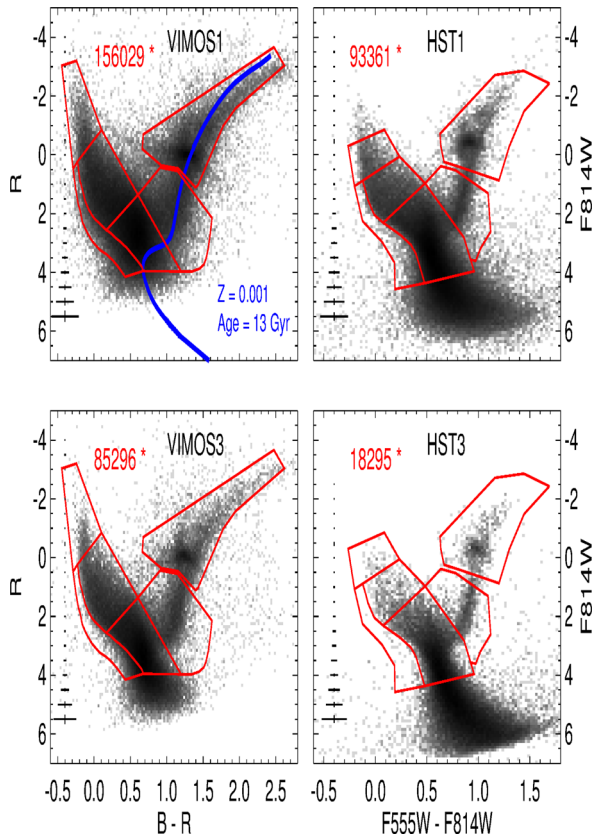


Figure 2. Left-hand panels: CMDs of two of the VIMOS fields which have a nearby mosaic of WFPC2 data. The blue line in the upper panel is a 13-Gyr-old BaSTI isochrone with $Z = 0.001$; it highlights that even in the most central, crowded field our photometry is deep enough to reach the oMSTO. Right-hand panels: CMDs of the WFPC2 fields spatially located next to VIMOS fields whose CMDs are displayed in the left-hand panels. Red lines delimit the bundles containing the stars we used for the SFH calculation. The numbers of stars inside the bundles are labelled. Error bars indicating photometric uncertainties as a function of magnitude are shown in each panel.

0.02 ($-2.3 \leq [\text{Fe}/\text{H}] \leq 0.004$, assuming $Z_{\odot} = 0.0198$). The BaSTI stellar evolution library (Pietrinferni et al. 2004, solar scaled, overshooting set) has been adopted. For the initial mass function (IMF) and the binary star distribution function $\beta(f, q)$, we used the same values as in Meschin et al. (2014): a binary fraction $f = 0.4$ and a mass ratio distribution $q > 0.5$. The IMF was taken from Kroupa (2002) and is given by $N(m)dm = m^{-\alpha} dm$, where $\alpha = 1.3$ for stars with mass $0.1 \leq m/M_{\odot} \leq 0.5$, and $\alpha = 2.3$ for $0.5 \leq m/M_{\odot} \leq 100$.

The incompleteness and photometric uncertainties due to the observational effects have been simulated in the synthetic CMD for each VIMOS and *HST* pointing based on the results of the corresponding artificial-star tests. In the case of the two bar fields, we identified areas with reddening larger than average and removed the corresponding stars from the CMD used to derive the SFH (approximately one third of the stars were removed for this reason). We verified, however, that the changes in the SFH when including these regions are minimal. No significant effect due to differential reddening could be noticed in the CMD of the disc fields. To obtain the SFHs, we used a new algorithm developed in PYTHON by one of us (EJB) (see Bernard et al. 2015, for some details on the algorithm). The same method was applied to all the VIMOS fields and three *HST* groups.

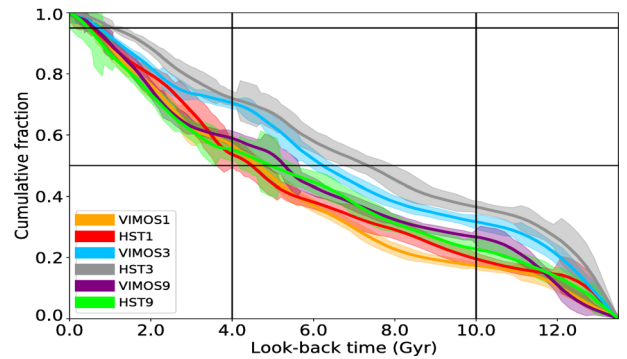


Figure 3. Comparison of the cumulative SFHs obtained from the VIMOS and WFPC2 data, for the three LMC regions for which the two data sources are available. The horizontal lines indicate mass fractions corresponding to 50 per cent and 95 per cent of the total accumulated mass. Vertical lines indicate the approximate ages which separate the main star-forming episodes mentioned in the text.

3.2 Comparison of VIMOS and *HST* SFHs

In this section, we compare the SFH of the two VIMOS fields located next to *HST* ones to show that the SFHs derived from the VIMOS data are compatible with those obtained from the deeper *HST* data. The results, in the form of cumulative SFHs, are displayed in Fig. 3. It can be seen that the SFHs for each VIMOS and corresponding WFPC2 field are basically identical within the errors, while there are noticeable differences between fields. The largest difference in photometric depth between the VIMOS and corresponding WFPC2 field occurs for the bar field (no. 1), for which the VIMOS CMD reaches just about half a magnitude below the oMSTO. The results in Fig. 3, however, show that the features in the SFH are equally recovered from both CMDs. The much larger number of stars in the less deep VIMOS CMD and, particularly, the fact that it does reach the oMSTO, are likely the key reasons for this.

3.3 The SFH of the LMC bar and inner disc from VIMOS data

We obtained SFHs for each individual VIMOS field and compared them. The detailed results on individual fields, including both $\text{SFR}(t)$ and age–metallicity relations, will be presented in a future paper (Monteagudo et al., in preparation). Disc field nos. 3, 4, 5, 6, 7, 8 and 10 have very similar SFHs, characterized by relatively smooth variations of the $\text{SFR}(t)$ with respect to a mean value, over the whole lifetime of the galaxy, resulting in a cumulative $\text{SFR}(t)$ close to a constant value. Therefore, for clarity in Fig. 3, we only show the SFH of field no. 3. The SFH of the two bar fields indicates a stellar population younger overall, while that of disc fields no. 9 and 11 (see SFH for field no. 9 in Fig. 3) is somewhat intermediate between the remaining disc fields and the bar fields. Since these two fields are located in the North LMC arm, we will exclude them from the upcoming analysis, focused on the comparison of the SFHs of the bar and inner disc. However, including them in the analysis would not change the conclusions of the Letter.

In this Letter, we are interested in exploring possible variations of the SFH within the bar, and between the bar and the surrounding inner disc fields. Therefore, for the purposes of this Letter, we have combined the CMDs of disc fields with similar SFHs into three CMDs which we will consider representative of the stellar populations of the inner disc in the N, E and SW directions. DiskE will correspond to fields with $\alpha_{2000} \geq 05:30:00$ (VIMOS4+6+10), DiskSSW to fields with $\alpha_{2000} \leq 05:10:00$ and $\delta_{2000} \geq -68:00:00$ (VIMOS3+7)

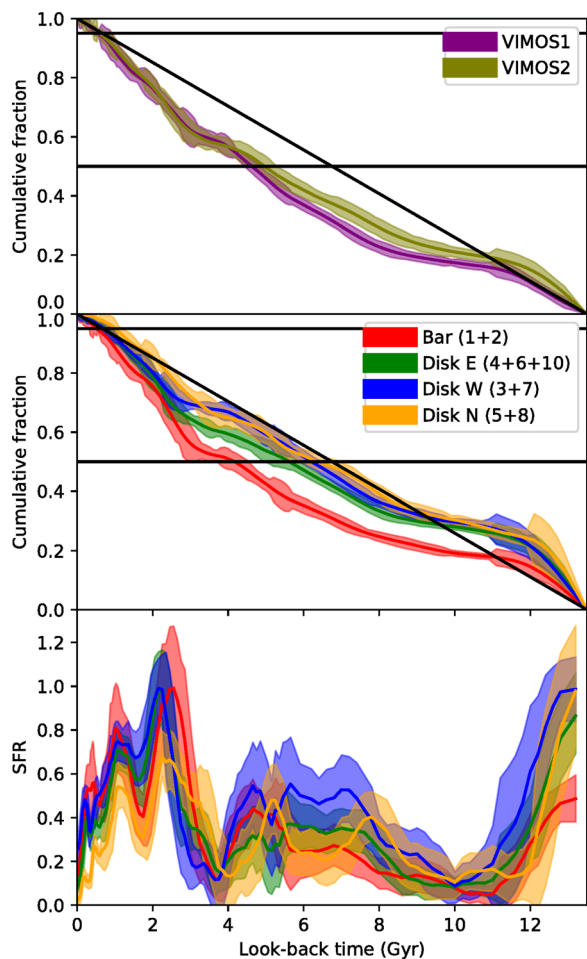


Figure 4. Top panel: cumulative SFHs for the LMC bar fields, no. 1 and no. 2. The horizontal lines indicate mass fractions corresponding to 50 per cent and 95 per cent of the total accumulated mass. Middle and lower panels: SFHs (in cumulative and time resolved forms, respectively) for the bar and disc fields, grouped as indicated in the text.

and DiskN to those with $\alpha_{2000} \simeq 05:14:00$ (VIMOS5+8). For the bar fields (nos. 1 and 2), we have computed individual SFHs, which are represented in the upper panel of Fig. 4 in the cumulative form. Note that both are almost identical within the errors (with the SFH for the central bar field marginally younger than that of the field in the NW extreme of the bar) indicating a basically common SFH for the whole bar. We have thus combined both bar fields for further comparison with the disc. These comparisons are shown in the middle and lower panels of Fig. 4 in cumulative and time resolved forms, respectively. In all figures, the SFHs are represented with their corresponding uncertainties, estimated following the prescriptions of Hidalgo et al. (2011).

The lower panel of Fig. 4 shows that the $SFR(t)$ of the bar and combined disc fields presents common features and consistent trends. All are characterized by three main periods of star formation separated by short gaps of almost negligible star formation activity. We find an early star formation episode (*old star-forming epoch*, O_{SFE}) common to all fields and lasting $\simeq 3.5$ Gyr. A second period of enhanced $SFR(t)$ (*intermediate star-forming epoch*, I_{SFE}) is found between 10 and 4 Gyr ago. Finally, the most recent period (*young star-forming epoch*, Y_{SFE}) began ~ 4 Gyr ago. Within each period, there are variations in the intensity of the $SFR(t)$ which are

Table 1. Derived values from the SFHs.

	Bar	Disc E	Disc SW	Disc N
Y_{SFE}	0.50 ± 0.03	0.40 ± 0.02	0.33 ± 0.02	0.35 ± 0.02
I_{SFE}	0.31 ± 0.03	0.31 ± 0.02	0.37 ± 0.03	0.34 ± 0.03
O_{SFE}	0.19 ± 0.02	0.28 ± 0.03	0.30 ± 0.03	0.30 ± 0.05
$(Y/O)_{SFE}$	2.6 ± 0.3	1.45 ± 0.18	1.12 ± 0.13	1.16 ± 0.21
$(Y/(I+O))_{SFE}$	1.00 ± 0.09	0.68 ± 0.05	0.49 ± 0.04	0.55 ± 0.07
T_{50} per cent (Gyr)	4.25	5.5	6.25	6.25
T_{95} per cent (Gyr)	0.5	0.75	0.75	1.00

only slightly different in detail from field to field. In particular, it is interesting to note that, within the young star-forming epoch, which is the one for which we can be most confident on the details of $SFR(t)$, there are variations that are totally consistent among all fields. Three peaks of star formation activity are observed at $\simeq 2.5$, 1.0 and 0.5 Gyr ago, while star formation appears very much reduced at the present time.

The difference between bar and disc fields is the relative number of stars formed in the three main epochs of star formation. In the first three lines of Table 1, we indicate the fraction of stars formed in each of them, for the combined bar fields and disc fields. The fraction of stars formed in the O_{SFE} is lower in the bar field than in the disc fields, and the contrary is true for the Y_{SFE} , while the fraction formed at intermediate ages is similar in all fields. This leads to a ratio Y/O and $Y/(I+O)$ about a factor of 2 larger in the bar compared to the disc. These differences are reflected in the respective cumulative mass fractions, displayed in the middle panel of Fig. 4. In this figure, the two horizontal lines indicate 50 and 95 mass percentiles. The ages at which these percentiles are reached in each field are listed in Table 1. They indicate that the disc formed half of its mass between 1.25 and 2 Gyr earlier than the bar.

3.4 Discussion: the origin of the LMC bar

The highly detailed SFHs which we have derived for a number of regions covering representative portions of the LMC bar and inner disc allow us to provide important constraints on the nature of the LMC bar. In the previous section, we have shown that the SFHs of the bar and disc fields closely share the same features, and thus, *no event of star formation can be identified with the formation of the LMC bar*. This conclusion is different from that reached in previous studies (Elson et al. 1997; Smecker-Hane et al. 2002). In particular, Smecker-Hane et al. (2002) identified a 4–6 Gyr star formation episode with the formation of the LMC bar. The significantly larger fields, covering different positions in the LMC inner regions, and the more sophisticated analysis technique (Smecker-Hane et al. 2002, simply modelled the main-sequence luminosity function to derive the SFH), makes us confident that our conclusion is robust. It implies that the bar likely formed from a redistribution of disc material which occurred when the disc became bar unstable, and shared a common SFH with the inner disc thereafter.

The fact that the Y_{SFE} has been somewhat more intense in the bar (and in its innermost region) than in the inner disc might be a consequence of younger, colder material and gas being preferentially funnelled to the centre of the galaxy by the non-axisymmetric potential. However, it may also simply be a continuation of the gradient seen in the outer disc (Gallart et al. 2008; Meschin et al. 2014), and common in dwarf irregular galaxies (e.g. Bernard et al. 2007; Stinson et al. 2009; Hidalgo et al. 2013) in the sense that younger

populations are concentrated towards the central parts of the galaxies.

The fact that the two bar fields, one located in its very centre and the other on its northern rim, also share a closely similar SFH that allows us to put further constraints on the characteristics of the LMC bar. Friedli & Benz (1995) showed that the formation of a strong bar in a typical Sc disc induces a significant starburst in the bar and in the Galactic Centre. The lack of an excess of $H\alpha$ emission in the bar region (Kim et al. 1999) indicates that such a starburst is not currently ongoing and our SFH results allow us to reach the same conclusion for the rest of the galaxy's lifetime. This kind of predicted variations of the SFH within the bar caused by bar formation and buckling have been recently observed in the SBb galaxy NGC 6032, where it was also observed that the SFH of the outer bar was similar to that of the disc (Pérez et al. 2017). The basically identical SFH across the LMC bar argues that these buckling mechanisms, which are characteristic of classical bars in more massive galaxies, are absent from the LMC and more generally from Sm type galaxies. This is in good agreement with recent simulation results (see Athanassoula 2016, for a review and references therein). A more comprehensive mapping of the SFH across the whole LMC bar is necessary to confirm this point, which places important constraints on the formation of bars in low mass galaxies, particularly of the Magellanic type.

ACKNOWLEDGEMENTS

We thank I. Pérez, I. Martínez-Valpuesta and T. Ruiz-Lara for interesting discussions, and an anonymous referee for useful suggestions that have helped us to improve the paper. This research is based on observations made with the European Southern Observatory (ESO) Very Large Telescope (VLT) at the La Silla Paranal Observatory under programme ID 084.B-1124 (PI: C. Gallart), in observations made with the NASA/ESA *Hubble Space Telescope (HST)*, obtained from the data archive at the Space Telescope Science Institute and on observations at Cerro Tololo Inter-American Observatory 4m-Blanco Telescope (NOAO Prop. ID: 2009B-0192; PI: M. Monelli), which is operated by AURA under a cooperative agreement with the National Science Foundation. STScI is operated by AURA under NASA contract NAS 5-26555. This work has been supported by the Spanish Ministry of Economy and Competitiveness under grant AYA2014-56795-P. EJB acknowledges support from the Centre National d'Études Spatiales (CNES) postdoctoral fellowship programme.

REFERENCES

Aparicio A., Gallart C., 2004, *AJ*, 128, 1465
 Aparicio A., Hidalgo S. L., 2009, *AJ*, 138, 558
 Athanassoula E., 2016, *Astrophysics and Space Science Library*, Vol. 418, Galactic Bulges, Springer-Verlag, Switzerland, p. 391

Bernard E. J., Aparicio A., Gallart C., Padilla-Torres C. P., Panniello M., 2007, *AJ*, 134, 1124
 Bernard E. J., Ferguson A. M. N., Chapman S. C., Ibata R. A., Irwin M. J., Lewis G. F., McConnachie A. W., 2015, *MNRAS*, 453, L113
 Cioni M.-R. L., Habing H. J., Israel F. P., 2000, *A&A*, 358, L9
 de Vaucouleurs G., Freeman K. C., 1972, *Vistas Astron.*, 14, 163
 Elson R. A. W., Gilmore G. F., Santiago B. X., 1997, *MNRAS*, 289, 157
 Friedli D., Benz W., 1995, *A&A*, 301, 649
 Gaia Collaboration et al., 2016, *A&A*, 595, A2
 Gallart C., Freedman W. L., Aparicio A., Bertelli G., Chiosi C., 1999, *AJ*, 118, 2245
 Gallart C., Stetson P. B., Meschin I. P., Pont F., Hardy E., 2008, *ApJ*, 682, L89
 Hidalgo S. L. et al., 2011, *ApJ*, 730, 14
 Hidalgo S. L. et al., 2013, *ApJ*, 778, 103
 Holtzman J. A. et al., 1999, *AJ*, 118, 2262
 Holtzman J. A., Afonso C., Dolphin A., 2006, *ApJS*, 166, 534
 Kim S., Staveley-Smith L., Dopita M. A., Freeman K. C., Sault R. J., Kesteven M. J., McConnell D., 1998, *ApJ*, 503, 674
 Kim S., Dopita M. A., Staveley-Smith L., Bessell M. S., 1999, *AJ*, 118, 2797
 Koerwer J. F., 2009, *AJ*, 138, 1
 Kroupa P., 2002, *Science*, 295, 82
 Lah P., Kiss L. L., Bedding T. R., 2005, *MNRAS*, 359, L42
 Meschin I., Gallart C., Aparicio A., Hidalgo S. L., Monelli M., Stetson P. B., Carrera R., 2014, *MNRAS*, 438, 1067
 Nikolaev S., Drake A. J., Keller S. C., Cook K. H., Dalal N., Griest K., Welch D. L., Kanbur S. M., 2004, *ApJ*, 601, 260
 Olsen K. A. G., 1999, *AJ*, 117, 2244
 Pérez I. et al., 2017, *MNRAS*, 470, L122
 Pietrinferni A., Cassisi S., Salaris M., Castelli F., 2004, *ApJ*, 612, 168
 Smecker-Hane T. A., Cole A. A., Gallagher J. S., III, Stetson P. B., 2002, *ApJ*, 566, 239
 Staveley-Smith L., Kim S., Calabretta M. R., Haynes R. F., Kesteven M. J., 2003, *MNRAS*, 339, 87
 Stetson P. B., 1987, *PASP*, 99, 191
 Stetson P. B., 1994, *PASP*, 106, 250
 Stinson G. S., Dalcanton J. J., Quinn T., Gogarten S. M., Kaufmann T., Wadsley J., 2009, *MNRAS*, 395, 1455
 Subramaniam A., 2003, *Bull. Astron. Soc. India*, 31, 413
 Subramaniam A., Subramanian S., 2009, *ApJ*, 703, L37
 van der Marel R. P., 2001, *AJ*, 122, 1827
 Weisz D. R., Dolphin A. E., Skillman E. D., Holtzman J., Dalcanton J. J., Cole A. A., Neary K., 2013, *MNRAS*, 431, 364
 Wilcots E. M., 2008, *Astrophys. Space Sci. Proc.*, 5, 69
 Zaritsky D., 2004, *ApJ*, 614, L37
 Zhao H., Evans N. W., 2000, *ApJ*, 545, L35

This paper has been typeset from a $\text{\TeX}/\text{\LaTeX}$ file prepared by the author.